PAPER

Effects of oscillating poloidal current drive on magnetic relaxation in the Madison Symmetric Torus reversed-field pinch

IOP Publishing Plasma Physics and Controlled Fusion
Plasma Phys. Control. Fusion 61 (2019) 045004 (14pp) https://doi.org/10.1088/1361-6587/aaf9e0

Effects of oscillating poloidal current drive on magnetic relaxation in the Madison Symmetric Torus reversed-field pinch

Zichao Li[1], K J McCollam[2], T Nishizawa[2], E Parke[2], J S Sarff[2], Z A Xing[2], Hong Li[1], Wandong Liu[1] and Weixing Ding[1]

[1] KTX Laboratory and Department of Modern Physics, University of Science and Technology of China, Hefei 230026, People's Republic of China
[2] Department of Physics, University of Wisconsin–Madison, Madison, Wisconsin 53706, United States of America

E-mail: lizch@mail.ustc.edu.cn

Received 1 November 2018, revised 7 December 2018
Accepted for publication 19 December 2018
Published 22 February 2019

Abstract

Magnetic relaxation behavior in reversed-field pinch (RFP) experiments on the Madison Symmetric Torus device is modified by oscillating poloidal current drive (OPCD). We observe that OPCD modulates the nonlinear magnetic fluctuation dynamics of the RFP as it modulates the equilibrium and its linear stability properties. In particular, OPCD can entrain the RFP's nonlinear magnetic relaxation cycle and can therefore modify the frequency of the discrete relaxation events called sawtooth crashes. These crashes, which are intermittent or quasiperiodic in standard RFP plasmas without oscillating voltages, can be entrained by OPCD to become nearly periodic. The entrainment of the RFP sawtooth cycle is investigated by varying OPCD amplitude and frequency, as well as plasma equilibrium magnetic field reversal. Impurity ion (C^{+4}) heating induced and modulated by OPCD is measured by ion Doppler spectrometry and is ascribed to the modulation of magnetic reconnection activity.

Supplementary material for this article is available online

Keywords: Madison Symmetric Torus (MST), reversed-field pinch (RFP), oscillating poloidal current drive (OPCD), magnetohydrodynamics (MHD), magnetic reconnection, magnetic self-organization, ion heating

(Some figures may appear in colour only in the online journal)

1. Introduction

The reversed-field pinch (RFP) configuration [1] is characterized by a poloidal magnetic field comparable in magnitude to the toroidal field, whose direction reverses near the plasma edge. Almost all of the field is produced by currents carried in the plasma itself. The standard RFP is sustained by a toroidal loop voltage, and its dynamics are governed by magnetic self-organization. Magnetic equilibrium profiles are determined by the interplay of the applied loop voltage, which drives parallel current peaked in the core, and a fluctuation-induced dynamo mechanism, which transfers current from the core to the edge during magnetic relaxation.

In standard RFP plasmas in the Madison Symmetric Torus (MST) experiment [2], such relaxation tends to occur as a quasiperiodic series of discrete relaxation events called sawtooth crashes, making up a sawtooth cycle recurring as follows. Typically, the innermost core-resonant tearing mode of poloidal mode number $m = 1$, which in MST is usually that with toroidal mode number $n = 6$, is the most unstable, i.e. it has the highest linear growth rate, due to free energy in the peaked equilibrium profile of normalized parallel current density $\lambda \equiv \mu_0 J_{\|}/B$. Edge-resonant $m = 0$ modes are typically observed to be linearly stable (or to have only very slow linear growth rates) in MST [3], likely due to conducting shell proximity [4]. As the $n = 6$ grows on time scales of order

1 ms, it interacts nonlinearly with other $m = 1$ modes, which also grow as energy is extracted from the equilibrium profile. At some instances, the amplitudes of all of these nonlinearly coupled $m = 0$ and $m = 1$ modes rapidly increase, on a $\sim$0.1 ms time scale, marking the onset of the sawtooth crash. The tearing modes generate a fluctuation-induced dynamo EMF that drives parallel current in the edge and suppresses it in the core, flattening the λ profile, which is magnetic relaxation. The crash ends with an abrupt decrease in tearing mode amplitudes driven by nonlinear coupling between modes, and then another sawtooth relaxation cycle period begins [5].

The sawtooth crash magnetic relaxation event corresponds to a release of magnetic energy with approximately conserved magnetic helicity [6], and an appreciable fraction of this energy is observed to be converted into ion thermal energy [7]. The nonlinear interactions of $m = 0$ and $m = 1$ tearing modes produce global magnetic reconnection which heats both impurity [8] and majority [9] ions. However, identification of the detailed mechanism or mechanisms responsible for ion heating in magnetic reconnection is a longstanding area of active research [10–15].

The magnetic reconnection inherent in the nonlinear tearing mode interactions of magnetic relaxation produces stochastic magnetic fields and strongly increases outward radial energy transport due to parallel streaming. To address this, pulsed poloidal current drive (PPCD) [16] was devised first on MST and later applied to other RFP experiments [17–19]. An inductive poloidal loop voltage pulse drives parallel current in the outer plasma, directly flattening the λ profile and stabilizing the core $m = 1$ tearing modes, suppressing the natural dynamo process of magnetic relaxation and providing a significant improvement in RFP energy confinement [20].

Exploiting magnetic reconnection to heat the ions in conjunction with PPCD was also found to be feasible. By controlling RFP equilibrium parameters to encourage large sawtooth crashes just before PPCD was applied, the increased ion thermal energy generated by the reconnection was captured by the improved confinement of PPCD [21]. Thus, the ability to control magnetic relaxation and therefore magnetic reconnection is of more general interest than merely that in suppressing it.

A limitation of PPCD is its transient character, as it relies on a monopolar voltage pulse. On the RFX device, Bolzonella *et al* investigated the feasibility of overcoming this by applying oscillating poloidal current drive (OPCD), which is an oscillating inductive poloidal loop voltage, thereby demonstrating a net energy confinement improvement due to this quasi-stationary current profile control technique [22]. In optimized cases, the improvement observed during the PPCD-like phase of OPCD outweighed a degradation during the anti-PPCD phase. OPCD experiments also showed it to be effective in producing quasi-single helicity (QSH) states, wherein the innermost, dominant $m = 1$ tearing mode amplitude increases markedly while the other, secondary $m = 1$ amplitudes decrease, which also has a positive effect on energy confinement [22, 23]. A similar state is observed in some nonlinear MHD simulations [24].

Applying an oscillating poloidal loop voltage is an integral component of oscillating-field current drive (OFCD) [25], which utilizes both poloidal and toroidal oscillations to inject net magnetic helicity [26] and drive quasi-steady current via magnetic relaxation, sustaining the RFP, as demonstrated in nonlinear MHD simulations [27]. This process was first tested experimentally in ZT-40M [28] and later in MST, where both a 10% plasma current increase [29] and a small confinement improvement [30] were observed due to the addition of OFCD to the background induction. Conceptually, OFCD has been envisioned as the most viable sustainment option for both steady-state [31] and hybrid inductive, pulsed-burn [32, 33] RFP reactor scenarios. Thus, as the application of OPCD bears on energy confinement and plasma sustainment, two fundamental aspects of RFP performance, studying OPCD may be helpful in advancing the RFP configuration.

From a basic physics perspective, OPCD provides a convenient way to study the nonlinear dynamics of self-organization, relaxation, and reconnection in a magnetized plasma. For example, one prominent issue in this context is the problem of reconnection triggering or onset [34], i.e. precisely identifying the causes of what are often explosive magnetic reconnection events observed in space, astrophysical, and laboratory plasmas including the RFP. We can help to investigate such fundamental questions through measuring the RFP plasma response to the oscillating external perturbations of OPCD, which is our present purpose.

In this paper, we report the results of MST experiments focused on two main physical effects of OPCD. The first is its modification of magnetic fluctuation and relaxation activity in the RFP, in particular its entrainment of the standard RFP sawtooth cycle. As opposed to the quasiperiodic cycle observed in the standard case, with OPCD, the crash events can be made nearly periodic, repetitive only near a particular phase of the OPCD cycle. We relate this to the overall magnetic relaxation process in terms of changes to the λ profile and its MHD stability properties, and therefore to magnetic tearing fluctuation dynamics and dynamo EMF, as modulated cyclically by the OPCD loop voltage. We present some aspects of this phenomenon as characteristics of RFP trajectories in equilibrium parameter spaces. The entrainment effect has been noted in previous oscillating-field experiments [29, 30, 35] but has not been tested before as systematically as it is here.

The second main effect is an observed modulation of impurity ion (C^{+4}) temperature by OPCD, the energy source for which we understand to be the magnetic energy released by the magnetic reconnection produced by nonlinear tearing mode interactions during the magnetic relaxation modulated by OPCD.

This paper is organized as follows. In section 2, the experimental setup and key diagnostics are described. Results on sawtooth entrainment by OPCD are presented in section 3. Section 4 describes the observed OPCD effects on impurity ion temperature. Finally, we further discuss these results and conclude in section 5.

2. Experimental setup and key diagnostics

The MST vessel has major radius $R_0 = 1.50$ m and minor radius $a = 52$ cm, with a limited plasma minor radius of about 50 cm. Its 5 cm thick aluminum shell, which is a good conductor on the experimental time scale of up to around 100 ms, has insulating gaps in the poloidal and toroidal directions to allow external power supplies access to the plasma. Unique among RFP experiments, the MST shell fulfills the roles of vacuum vessel, single-turn toroidal field coil, and close-fitting conducting shell, the last of which is important for the linear stability of the $m = 0$ modes discussed in this paper. The results described below come from a series of RFP shots in deuterium plasma each with or without OPCD applied. In either case, the standard toroidal induction to sustain the RFP is supplied by a pulse-forming network in MST's poloidal magnetic field circuit. A programmable power supply (PPS) [36] in MST's toroidal magnetic field circuit provides poloidal current in the shell, which serves as the toroidal field coil, and this helps maintain standard field reversal as well as the oscillating loop voltage in OPCD cases. Apart from modulations and slow secular changes due to OPCD in those cases, plasma current I_p is maintained at about 250 kA. Depending on the experiment, the central chord-average electron density n_e measured by a CO_2 interferometer ranges from several $10^{18}\,m^{-3}$ to about $10^{19}\,m^{-3}$ during discharge flattops.

Three other parameters are varied shot-to-shot for the experiments presented below using the PPS: the flattop value of RFP reversal parameter and the OPCD amplitude and frequency. Note that the RFP equilibrium state can be characterized by two measured dimensionless parameters: reversal parameter $F \equiv B_\phi(a)/B_{\phi,\,\mathrm{ave}}$, where $B_\phi(a)$ is the toroidal field at the wall and $B_{\phi,\,\mathrm{ave}}$ is the cross-sectional average toroidal field (measured by a flux loop), and pinch parameter $\Theta \equiv B_\theta(a)/B_{\phi,\,\mathrm{ave}}$, where $B_\theta(a)$ is the poloidal field at the wall. Depending on the experiment, the flattop- or OPCD cycle-average $\langle F\rangle$ value ranges from about -0.05, shallow reversal, to about -0.35, moderately deep reversal, where -0.2 is typical for standard RFP operation in MST. The chosen OPCD amplitudes A_{osc} correspond to approximately either the absolute value $|\langle F\rangle|$, $|\langle F\rangle|/2$, or $|\langle F\rangle|/4$. For some full-amplitude OPCD shots ($A_{\mathrm{osc}} \approx |\langle F\rangle|$), F values might briefly reach above $F = 0$, which is to say the plasma momentarily goes out of reversal due to the large OPCD amplitude, but this does not seem to significantly affect the dynamics, and F is quickly taken back to negative values by the applied poloidal loop voltage. The OPCD oscillation frequency f_{osc} is scanned over several values from 69 to 1100 Hz. The OPCD pulse is always begun at the same shot time, 20.0 ms, and the OPCD duration is 17.5 ms.

Actively integrated magnetic fluctuation signals from a toroidal array of edge B-dot coils are spectrally resolved into toroidal mode numbers n, with toroidal and poloidal component amplitudes $\widetilde{B}_{\phi,n}$ and $\widetilde{B}_{\theta,n}$, respectively, via discrete spatial Fourier transforms. By the polarization properties of resonant modes in the RFP, we infer the dominant poloidal mode number $m = 0$ or $m = 1$ for each n mode. In particular, combining the resonance condition $q = m/n$ on the safety factor q, derived from $\mathbf{k}\cdot\mathbf{B} = 0$ for the mode wave vector $\mathbf{k}$ and equilibrium field $\mathbf{B}$, with the fact that $q < 1/4$ is true for RFPs in MST implies that the minimum n value of $m = 1$ modes is $n = 5$. Also, the condition of zero radial current at the plasma edge is given by $\mathbf{k}\times\widetilde{\mathbf{B}} = 0$, or $na\widetilde{B}_\theta = mR\widetilde{B}_\phi$, in a cylindrical approximation implying that our edge coils do not detect a θ component for $m = 0$ modes. Accordingly, we use $\widetilde{B}_{m=0} \equiv \sqrt{\sum_{1\leqslant n\leqslant 4}\widetilde{B}^2_{\phi,n}}$ as an indicator of $m = 0$ magnetic fluctuation amplitude and $\widetilde{B}_{m=1} \equiv \sqrt{\sum_{5\leqslant n\leqslant 15}\widetilde{B}^2_{\theta,n}}$ for $m = 1$.

Time-resolved, chord-average C^{+4} impurity ion temperatures T_{C+4} are measured by analyzing line emission signals around 227.1 nm detected by the ion Doppler spectroscopy (IDS-II) diagnostic [37]. The T_{C+4} data serves as a proxy for the majority ion (D^+) temperature, as collisional equilibration times between the two species in our plasma cases are less than about 0.1 ms. Ten poloidal viewing chords are used, with the capability of using two chords simultaneously, changeable on a shot-by-shot basis. Two chords, whose impact parameters are 6 cm outboard ($r/a = +0.11$) and 40 cm inboard ($r/a = -0.76$) of the geometric axis, are used to provide chord-averaged ion temperature signals for the core and edge, respectively. Radial profiles of C^{+4} emission intensities are broad for the MST plasmas used in this work, such that we assume chord impact parameters roughly reflect the true radial location of the observed C^{+4} temperatures. Note that even this rough localization would not be possible if the emission profile were narrow, as it is in some other MST experiments at higher temperatures than those considered here. Because the RFP equilibrium magnetic field is dominantly toroidal in the plasma core and poloidal at the edge, the poloidal viewing chords preferentially detect perpendicular temperatures $T_\perp$ for core chords and parallel temperatures $T_\parallel$ for edge chords.

Time-resolved, chord-average electron density profiles are measured with a far-infrared (FIR) interferometer system having 11 vertical viewing chords [38]. The interferometer sampling frequency is 6 MHz, and the calculated density data frequency is about 750 kHz.

For all of the diagnostics used for measurements presented in this work, measurement uncertainties are small compared to the observed shot-to-shot variations in the measured quantities. For each uncertainty estimate for an ensemble-averaged result, we use the standard error $\sigma/\sqrt{N}$ of the mean value, i.e. the standard deviation σ over the square root of the number N of events in the ensemble.

3. Sawtooth entrainment

OPCD entrains sawtooth magnetic relaxation events by directly modulating the current profile. In figure 1, time series of several plasma quantities for the flattop of a standard RFP pulse in the left-hand column are compared to about five periods of an OPCD pulse with $f_{\mathrm{osc}} = 275$ Hz on the right. In both cases, the average flattop reversal value is $\langle F\rangle \approx -0.2$, and full-amplitude oscillations ($A_{\mathrm{osc}} \approx |\langle F\rangle|$) are applied in

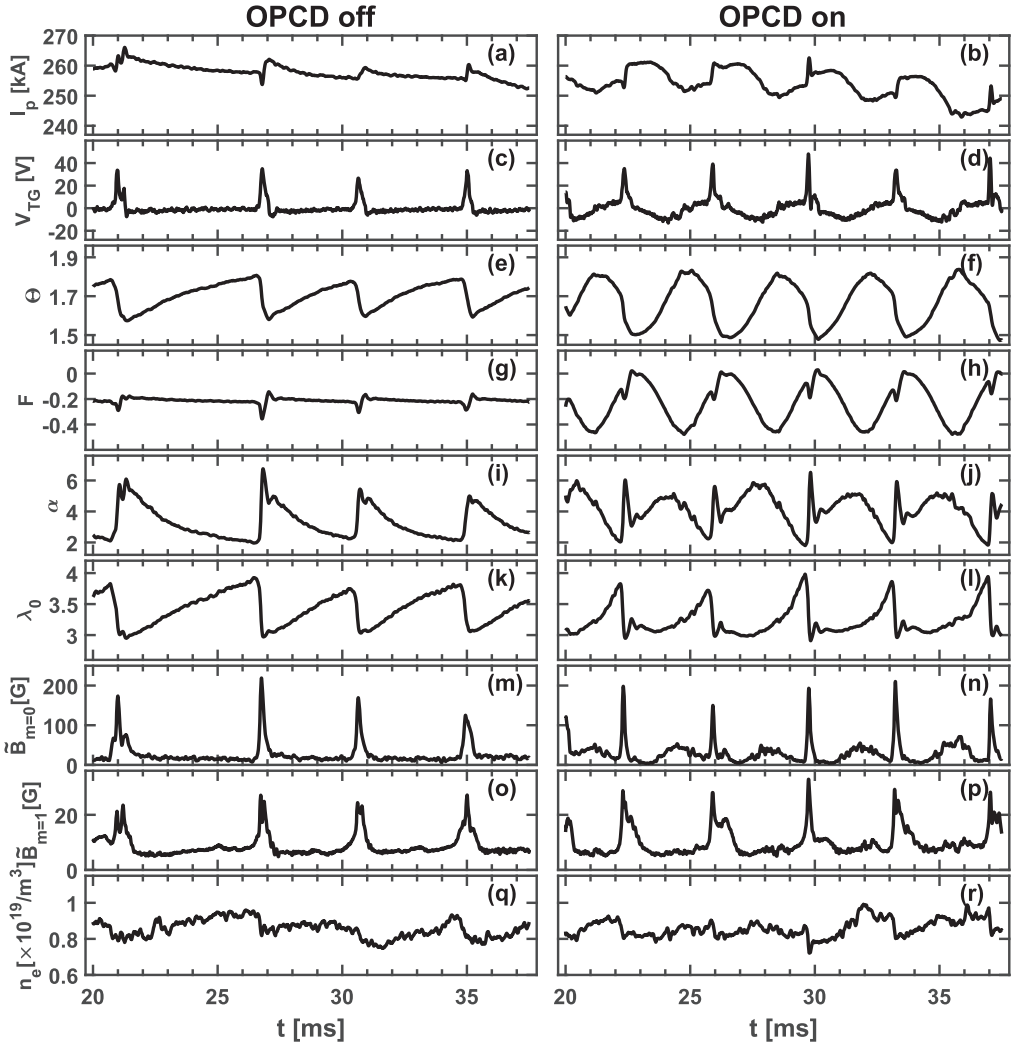

Figure 1. Time evolution during a standard, OPCD off discharge at $\langle F \rangle \approx -0.2$ (left column) and an OPCD pulse at $f_{\rm osc} = 275$ Hz, full-amplitude $A_{\rm osc} \approx 0.2$, and $\langle F \rangle \approx -0.2$ (right column): (a), (b) plasma current $I_{\rm p}$; (c), (d) poloidal loop voltage $V_{\rm TG}$; (e), (f) pinch parameter Θ; (g), (h) reversal parameter F; (i), (j) λ-profile parameter α; (k), (l) λ-profile parameter λ_0; (m), (n) $m = 0$ ($1 \leqslant n \leqslant 4$) and (o), (p) $m = 1$ ($5 \leqslant n \leqslant 15$) edge magnetic fluctuation amplitudes $\widetilde{B}_{m=0}$ and $\widetilde{B}_{m=1}$; (q), (r) central chord-average electron density $n_{\rm e}$.

the OPCD case. The amplitude of the OPCD loop voltage across the toroidal gap ($V_{\rm TG}$) is about 10 V.

For the standard shot, there are four sawtooth crashes in this example, while there are five distinct crash events during OPCD, one per period. The crashes are identifiable as the sharp spikes in $V_{\rm TG}$, which are induced by plasma relaxation in either case, rather than directly by an external power supply. Typical durations of the crash events themselves are of order hundreds of microseconds in either the standard or OPCD case. In the standard case, the crashes are quasiperiodic, but in the OPCD case, they are entrained to occur only around a certain phase of each OPCD cycle and are therefore nearly periodic if occurring once per period as in this example.

The timing of sawtooth crashes can be described in terms of the λ profile and $m = 0$ and $m = 1$ tearing mode activity. Through a simple cylindrical equilibrium model called the 'alpha model' [39], the measured values of Θ and F are used to derive the profile parameters in the assumed λ profile, $\lambda_0\,[1 - (r/a)^{\alpha}]$, where λ_0 is the core value, and α is a flatness parameter that is larger for flatter profiles. The model includes finite pressure, and we assume a quadratic pressure profile, such that the poloidal beta $\beta \equiv 2\mu_0 p_{\rm ave} \,/\, {\rm B_p}(a)$ is fixed at 7%. We also make a small, order $< 1\%$ toroidal correction to the cylindrically modeled fields to account for the $\sim$1 cm edge vacuum region between the last closed flux surface and edge magnetic measurements. Time series of λ_0 and α appear in figure 1.

Focusing on the standard case, the large positive changes in α and negative changes in λ_0 during sawtooth crashes show their λ-flattening effect. After a crash, the steady toroidal loop voltage acts to peak up the λ profile on a typical time scale of several milliseconds, indicated by α decreasing and λ_0 ramping upward. Then, after about 1 ms of growth of evidently unstable $m = 1$ modes, roughly when α reaches about 2 and λ_0 about 4, both the $m = 1$ and $m = 0$ mode amplitudes spike up sharply as the next crash in the sawtooth cycle occurs. This is a quasiperiodic process. Although we

can observe the approximate conditions leading to a crash in the standard RFP, we have not identified precise triggering conditions, and only its average timing over many cycles is predictable. The experimentally observed scaling of this sawtooth period on plasma parameters [40] is in agreement with earlier nonlinear MHD simulations [41].

In the OPCD case in figure 1, the oscillating poloidal loop voltage is added to the same steady toroidal loop voltage applied in the standard case. This produces an oscillation in I_p, a consequence of the inherent coupling in the RFP between toroidal and poloidal fields. The OPCD also directly modulates the λ profile on the oscillation cycle time scale through inductive current drive. Near the end of each OPCD half-cycle with applied voltage in the anti-PPCD sense, α reaches about 2 and λ_0 about 4, i.e. the λ profile becomes very peaked due to poloidal anti-current drive, around which time a crash occurs, accompanied by sharp spikes in $m = 1$ and $m = 0$ mode amplitudes as in the standard case. After the crash, during the co-PPCD half-cycle, the applied current drive initially has a PPCD-like effect, flattening the λ profile and suppressing mode amplitudes. Soon, however, still during the co-PPCD phase and well before the next sawtooth crash, mode amplitudes, particularly for $m = 0$, start to increase to quite large amplitudes (up to about 50 G for $m = 0$ in figure 1), even though the λ profile is still quite flat ($\alpha \approx 4$, $\lambda_0 \approx 3$). Large mode amplitude excursions similar to these are also observed in over-driven PPCD [42] and in some OFCD conditions [30], where they are thought to be due to linear $m = 0$ instability rather than $m = 1$ instability as they would be in a sawtooth crash.

To confirm the robust effects of OPCD, sawtooth ensemble-average results are also shown in figure 2. Using ensembles of time windows around many sawtooth crash events with similar plasma conditions, we average over the data with each time window referenced to its corresponding sawtooth crash. The time window duration chosen for this ensemble data is 3.6 ms, roughly the OPCD period. This analysis underscores that the main effect of OPCD is to add oscillatory components to entrained sawtooth crashes that by themselves are similar to the crashes typical of a standard RFP.

The λ profile and mode activity in RFP relaxation can be related through the concept of MHD stability. Though relaxation is a nonlinear process, considering linear stability may help identify the modes responsible for extracting energy from the equilibrium and help elucidate how the sawtooth crash is triggered. Antoni *et al* calculated ideal and resistive stability properties for $m = 0$ and $m = 1$ modes in zero-beta, cylindrical RFPs with no edge vacuum region and which were characterized by alpha model profiles [39]. For the equilibrium F values relevant to our experiments, internal $m = 1$ modes were found to be the limiting instabilities, in that $m = 0$ modes are stable in these cases. Using their $m = 1$ stability diagram in (α, $\Theta_0 \equiv \lambda_0 /2$) space as a background, we overplot an ensemble of MST data points from just before and just after many sawtooth crashes, i.e. the 'starting' and 'stopping' times, for both standard and OPCD shots in figure 3. To identify these time points efficiently, we first identify each crash event automatically, using an empirically determined critical threshold value of the proxy $\widetilde{B}_{m=0}\widetilde{B}_{m=1}$, which we find does a good job of discriminating crashes from other types of magnetic activity. For each event, within a time window depending on the proxy superceding the threshold, we identify the starting and stopping times as the times of maximum F values just before and after the maximum proxy value.

In figure 3, one can clearly see that crashes overwhelmingly tend to occur when the λ profile is well inside the region of instability for an internal $m = 1$ mode, whether resistive or ideal, and the crashes usually take the RFP into the region completely stable to $m = 1$. Both standard and OPCD data appear similar to each other in this sense, with little to distinguish between them, suggesting that the same $m = 1$ physics is operative around the crash in both cases. We emphasize that this aspect of crash behavior with respect to $m = 1$ linear stability does not imply that the crash is a linear phenomenon. In particular, while it has been hypothesized with some support in MHD simulations that a straightforward linear instability criterion is required in order for a crash to occur [43], it is apparently not the case that simply crossing a particular $m = 1$ stability boundary tends to trigger a crash.

There are some crash destination points in the unstable region in figure 3, and the significance of this is unclear. Perhaps these represent partial or incomplete relaxation events in some sense. Again, more fundamentally, magnetic relaxation is a nonlinear phenomenon, and there is no simple correspondence between the dynamics of several nonlinearly interacting modes and their simultaneous individual linear stability properties. It should also be remembered that the MST plasma does not satisfy all of the approximations of Antoni *et al* [39], since it has finite beta, toroidal geometry, and an edge vacuum region. Moreover, the alpha model is only an idealization of the actual current profile, which we are not measuring.

Examining the detailed trajectories of single-shot flattop time series in a 2D parameter space of the equilibrium parameters Θ and F is illustrative of the general features of profile modifications and sawtooth relaxation processes with and without OPCD, as in figure 4. As seen in figure 4(a), an example of a standard RFP case with $\langle F \rangle \approx -0.2$, during a sawtooth cycle, over the time span of several milliseconds at a roughly constant F value, the steady toroidal loop voltage moves the RFP to higher Θ values, corresponding to more peaked modeled λ profiles more unstable to $m = 1$ activity, i.e. having more positive $m = 1$ linear growth rates. At some point, the sawtooth crash quickly moves the RFP back to a low-Θ point via an intermediate swing into deeper F values, and the process repeats. Overall, the standard RFP executes a clockwise-oriented trajectory in (Θ, F) space. Conceivably, this path might be related to a limit cycle from nonlinear dynamics [44].

In OPCD cases, to the same steady motion toward higher Θ are added oscillations in both the F and Θ directions, as well as the entrained sawtooth crashes, and thus here, the trajectories are more complicated. Notably, at high OPCD amplitudes, (Θ, F) trajectories are observed to be

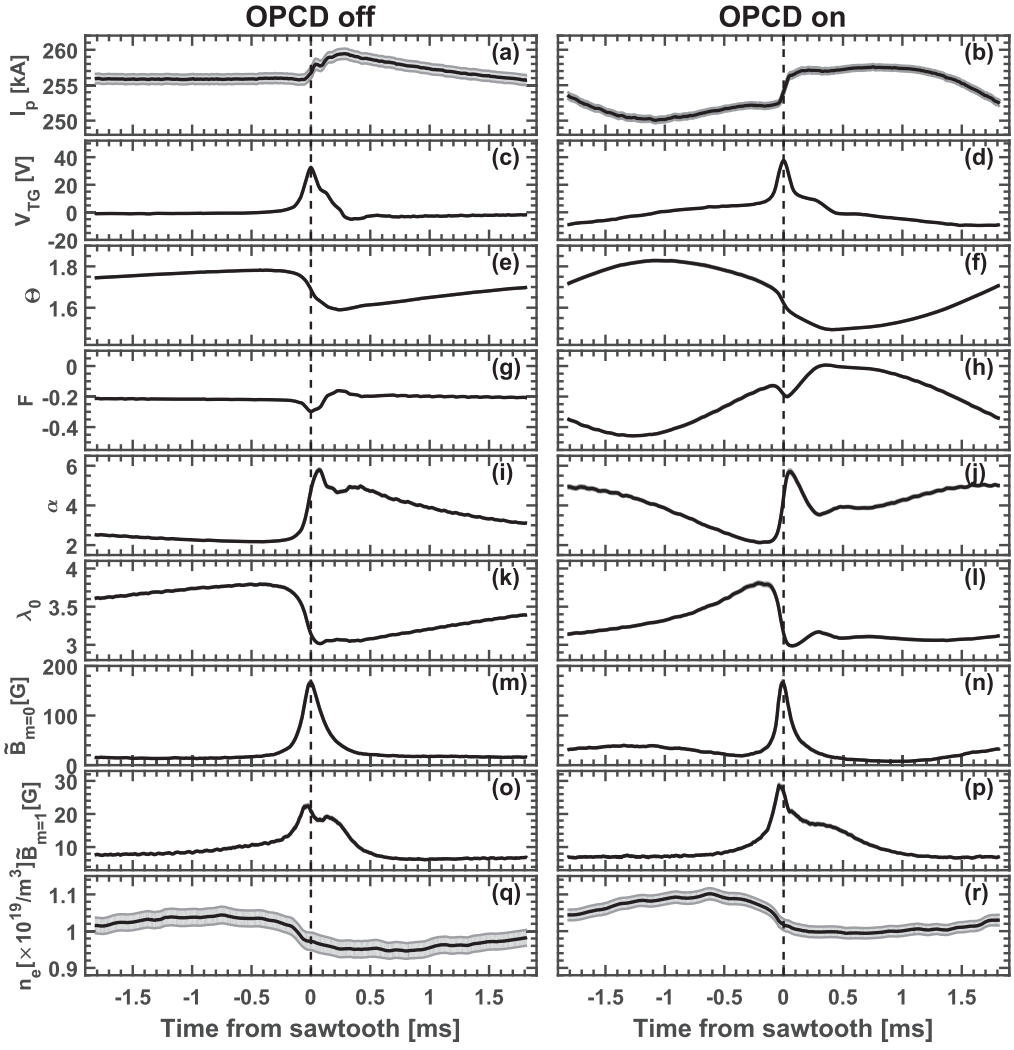

Figure 2. Ensemble-average time evolution during standard, OPCD off discharges at $\langle F\rangle \approx -0.2$ (left column) and OPCD pulses at $f_{osc} = 275$ Hz, full-amplitude $A_{osc} \approx 0.2$, and $\langle F\rangle \approx -0.2$ (right column): (a), (b) plasma current I_p; (c), (d) poloidal loop voltage V_{TG}; (e), (f) pinch parameter Θ; (g), (h) reversal parameter F; (i), (j) λ-profile parameter α; (k), (l) λ-profile parameter λ_0; (m), (n) $m = 0$ ($1 \leqslant n \leqslant 4$) and for (o), (p) $m = 1$ ($5 \leqslant n \leqslant 15$) edge magnetic fluctuation amplitudes $\widetilde{B}_{m=0}$ and $\widetilde{B}_{m=1}$; (q), (r) central chord-average electron density n_e. Shaded error bars (some of which are too small to see) represent standard errors $\sigma/\sqrt{N}$ of ensemble-average values, where $N = 104$ for OPCD off and 85 for OPCD on.

counterclockwise in sense overall, opposite to the standard case, though the shape of the crash trajectory itself remains roughly the same. An example of this is shown in figure 4(b), which is an OPCD case with $f_{osc} = 275$ Hz, full-amplitude $A_{osc} \approx 0.2$, and $\langle F\rangle \approx -0.2$, where the mostly counterclockwise trajectory is very clear. The (Θ, F) points where the two sawtooth crashes start and stop are located at almost the same position, emphasizing the strong entrainment effect. At a higher OPCD frequency of $f_{osc} = 550$ Hz and lower amplitude of $A_{osc} \approx 0.1$, as shown in figure 4(c), there are two OPCD cycles between entrained sawtooth crashes, and the RFP executes a double-loop trajectory between them. At a lower OPCD frequency of $f_{osc} = 138$ Hz and half-amplitude $A_{osc} \approx 0.1$, as shown in figure 4(d), trajectories tend to become quite complicated, in part as under these conditions, sawtooth crash entrainment is not as strong.

Sawtooth entrainment allows the possibility of controlling sawtooth frequency via OPCD and thus can play a role in controlling magnetic relaxation behavior. If there is one entrained sawtooth crash per OPCD cycle, then the crashes are nearly periodic, as in our previous OPCD example of figure 1. However, we find that if, starting from such a condition, the OPCD frequency is increased, then the entrained crashes need not remain periodic, because they tend to begin skipping cycles. The general situation is summarized in figure 5 for $\langle F\rangle \approx -0.2$, showing the crash frequency f_{crash} versus the OPCD frequency f_{osc} for different OPCD amplitudes A_{osc}. Note that the intrinsic crash frequency f_{int} for the standard RFP without OPCD is around 250 Hz (at $I_p \approx$ 250 kA and $n_e \approx 10^{19}$ m^{-3}), as also shown in figure 5. For f_{osc} values lower than this, while f_{crash} is about the same or smaller than f_{int}, there is, on average, more than one crash per OPCD period, a reflection of the weak entrainment in these cases, regardless of OPCD amplitude. For instance, in full-amplitude OPCD at $f_{osc} = 69$ or 138 Hz, sawteeth remain quasiperiodic, which is reflected in the rather large uncertainties in

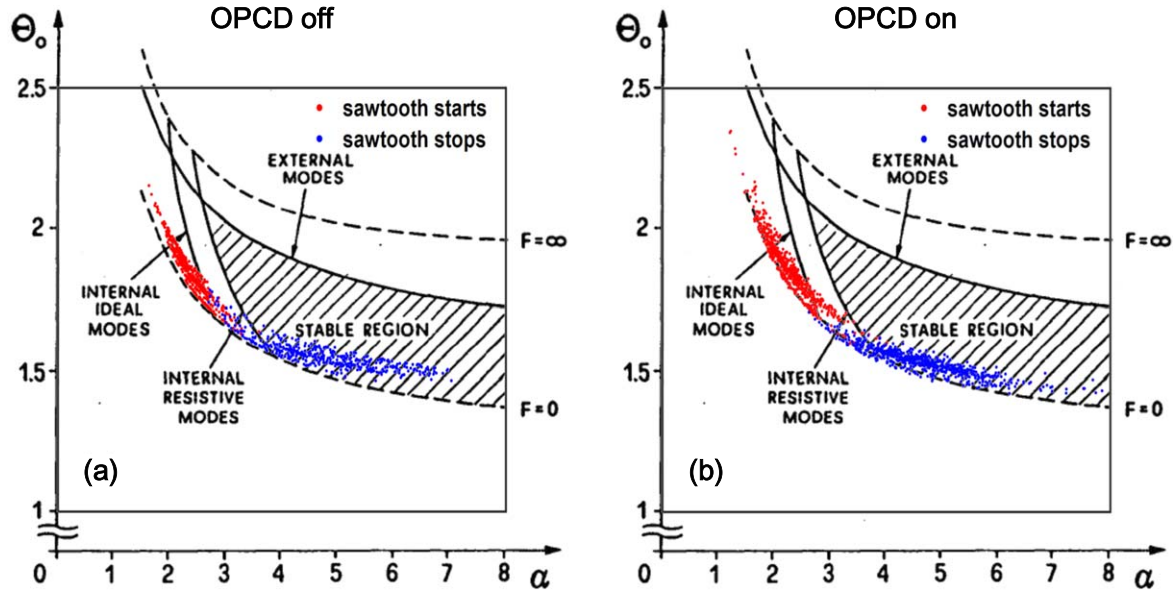

Figure 3. MST sawtooth crash data in (α, $\Theta_0 \equiv \lambda_0 / 2$) space plotted over $m = 1$ mode stability. (a) Standard RFP sawtooth crash starting (red) and stopping (blue) points for many sawtooth crash events; (b) same for OPCD crash events. Reproduced courtesy of IAEA. Figure from [39]. Copyright 1986 IAEA.

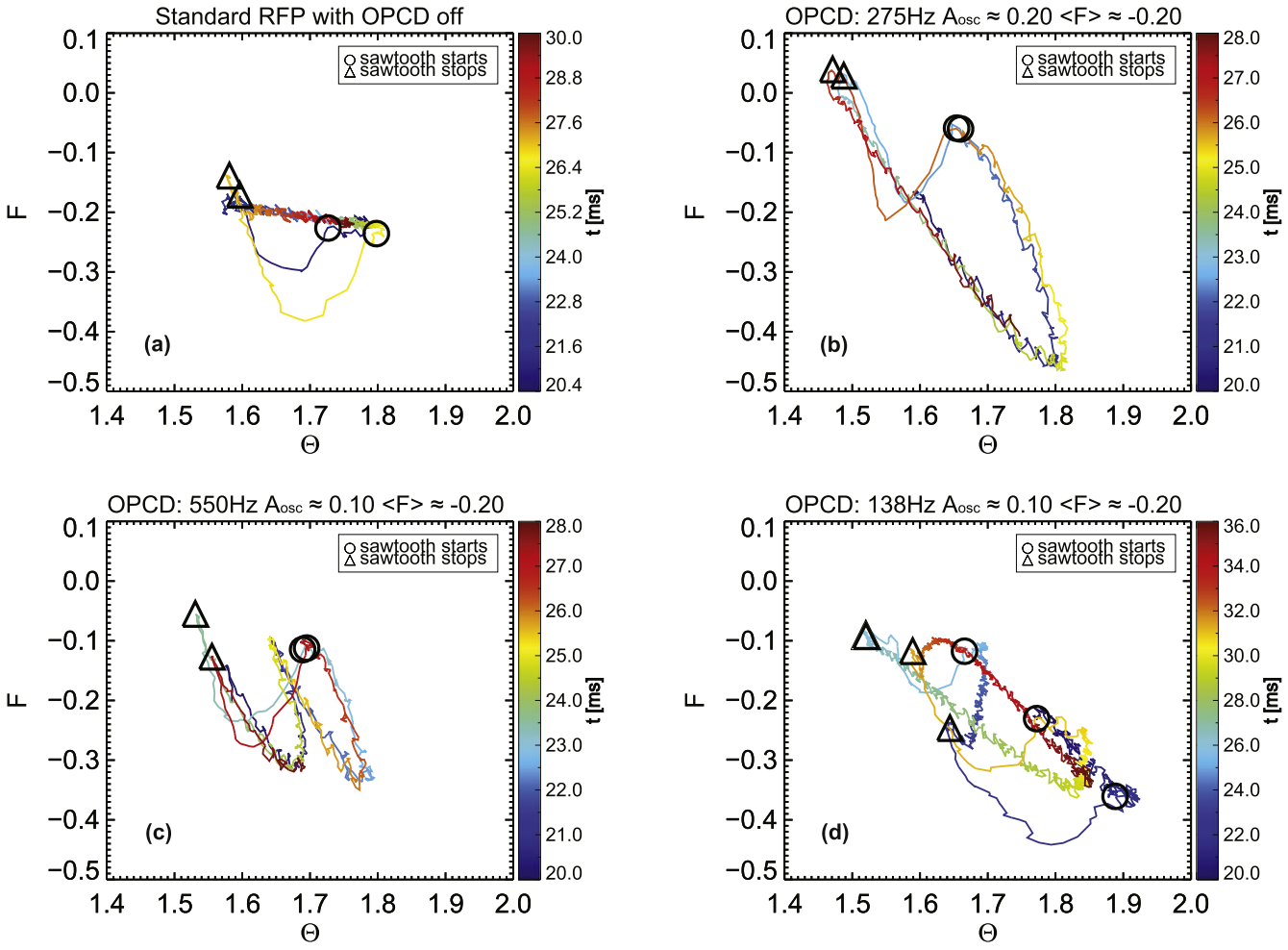

Figure 4. Sawtooth cycle trajectories in (Θ, F) space for four cases: (a) standard RFP with OPCD off, (b) OPCD at $f_{\mathrm{osc}} = 275$ Hz, full-amplitude $A_{\mathrm{osc}} \approx 0.2$, and $\langle F \rangle \approx -0.2$, (c) OPCD at $f_{\mathrm{osc}} = 550$ Hz, half-amplitude $A_{\mathrm{osc}} \approx 0.1$, and $\langle F \rangle \approx -0.2$, (d) OPCD at $f_{\mathrm{osc}} = 138$ Hz, half-amplitude $A_{\mathrm{osc}} \approx 0.1$, and $\langle F \rangle \approx -0.2$. Color maps indicate increasing time from blue to red. Black circles and triangles indicate sawtooth crash starting and stopping times, respectively.

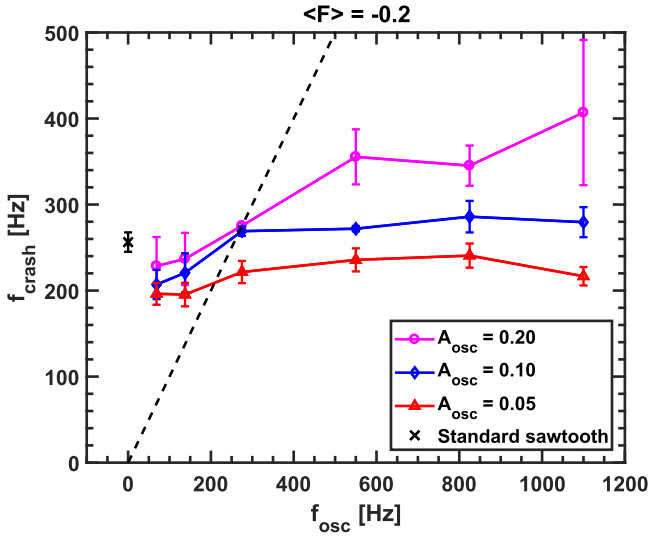

Figure 5. Ensemble-average sawtooth crash frequency f_{crash} versus OPCD frequency f_{osc} for different OPCD amplitudes A_{osc} (with $\langle F\rangle \approx -0.2$), compared to f_{int}, the crash frequency for the standard RFP without OPCD (black cross) at $I_{\mathrm{p}} \approx 250$ kA, $n_{\mathrm{e}} \approx 10^{19}\ \mathrm{m}^{-3}$, and $\langle F\rangle \approx -0.2$. The dashed line represents $f_{\mathrm{crash}} = f_{\mathrm{osc}}$. Error bars represent standard errors $\sigma/\sqrt{N}$ of ensemble-average values, where $N = 14$ for each case.

f_{crash}, as the oscillating loop voltage drives multiple crashes during each anti-PPCD half-cycle. At $f_{\mathrm{osc}} = 275$ Hz, which is in the neighborhood of f_{int}, for the OPCD amplitudes of $A_{\mathrm{osc}} \approx 0.1$ or 0.2, we observe $f_{\mathrm{crash}} \approx \mathrm{f_{osc}}$, meaning one crash per OPCD cycle. The crashes become quite strictly periodic, as evidenced by the small error bars on the points intersecting the dashed line in figure 5. For the full-amplitude case of $A_{\mathrm{osc}} \approx 0.2$ at higher f_{osc}, the f_{crash} values are well above f_{int}. The uncertainties in f_{crash} also tend to become relatively large in this limit, perhaps in part because entrainment is hampered by the higher-frequency oscillation's shallower penetration of the equilibrium. In the same limit, the middle amplitude case of $A_{\mathrm{osc}} \approx 0.1$ shows saturated values of f_{crash} of around 280 Hz, slightly above f_{int}. Regardless of frequency, the low amplitude case of $A_{\mathrm{osc}} \approx 0.05$ does not achieve mean f_{crash} values above f_{int}.

4. Ion heating

The application of OPCD is observed to cyclically modulate measured C^{+4} impurity ion temperatures $T_{\mathrm{C+4}}$, such that significant excursions occur between the entrained sawtooth crashes. This is in contrast to MST's standard RFP, wherein a large majority of the ion heating only occurs during sawtooth crashes. Figure 6 shows time series for a standard RFP pulse without OPCD and for a full-amplitude ($A_{\mathrm{osc}} \approx |\langle F\rangle|$) OPCD pulse, both at a relatively deep average reversal of $\langle F\rangle \approx -0.35$. Between crashes, OPCD-correlated excursions of order several tens of eV in core-chord $T_{\mathrm{C+4}}$ values and a few tens of eV in edge-chord $T_{\mathrm{C+4}}$ at around $f_{\mathrm{osc}} = 275$ Hz are clearly visible (though nonsinusoidal), in contrast to the standard shot, where ion heating is markedly smaller between sawteeth. This OPCD pulse is chosen for showing obvious $T_{\mathrm{C+4}}$ modulations in both core- and edge-chord signals. Over many pulses, such core-chord modulations are typical, but edge-chord modulations are typically smaller, as discussed below.

Simultaneous OPCD modulations in $\widetilde{B}_{m=0}$ and $\widetilde{B}_{m=1}$ magnetic fluctuation amplitudes are also obvious, and their peak values between entrained sawtooth crashes are of the same order as those during the crashes themselves. Such multimode magnetic activity is indicative of magnetic reconnection due to coupled tearing fluctuations. Note that this ion heating and magnetic activity are much more intense in this higher-amplitude OPCD case of $A_{\mathrm{osc}} \approx |\langle F\rangle| \approx 0.35$ than in the lower amplitude case of $A_{\mathrm{osc}} \approx |\langle F\rangle| \approx 0.2$ discussed in section 3 (figures 1 and 2). The total equilibrium magnetic energy $W_{\mathrm{mag}} \equiv \int B^2 \mathrm{d}V/(2\mu_0)$ as determined from alpha modeling is shown to drop noticeably during the peaking of $T_{\mathrm{C+4}}$, whether in a standard or OPCD plasma. Thus, in accordance with previous studies of ion heating in RFPs [7–9, 14], these observations indicate that the energy going into heating the ions comes from the magnetic equilibrium and that the heating mechanism relies on magnetic reconnection, evidenced here as multimode edge magnetic fluctuation amplitudes.

The OPCD-correlated excursions in $m = 0$ and $m = 1$ fluctuations between sawtooth crashes like those in figure 6 present an interesting aspect of multimode dynamics in the RFP. For OPCD cases generally similar to the examples in both figures 1 and 6, with $f_{\mathrm{osc}} = 275$ or 550 Hz, $\langle F\rangle$ ranging from -0.2 to -0.35, and full oscillation amplitudes A_{osc}, the n spectra of both of these $m = 0$ and $m = 1$ features tend to be multi-helicity (MH), i.e. to have significant mode energies at several n values. However, for cases with lower f_{osc}, as well as some cases with higher f_{osc} and lower A_{osc}, we observe tendencies for $m = 1$ spectra to become dominated by a single n mode, usually $n = 6$. This possibility for either MH or single-n-mode-dominated $m = 1$ states in OPCD experiments on MST is reminiscent of similar observations on RFX [22, 23]. The MST cases at lower f_{osc} also appear similar to some PPCD experiments on MST that evidence QSH-like spectra [45], in that the OPCD phenomenon occurs during the PPCD-like phase of the oscillating loop voltage. However, we emphasize that these single-n-mode-dominated $m = 1$ states in OPCD occur along with strong $m = 0$ activity, unlike the PPCD cases.

In figure 6, I_{p} and n_{e} show a secular decrease during the OPCD pulse, a typical result for MST experiments with high OPCD amplitudes. It is presumably accountable to a secular decrease in electron temperature T_{e} due to radial energy transport by stochastic magnetic fields during the large tearing mode increases between sawteeth. Measurements of T_{e} have not been made in MST OPCD plasmas, but in OFCD anti-current drive cases with similar secular I_{p} decreases, such measurements show marked T_{e} decreases [30]. Both the OPCD-modulated peaks and the entrained sawtooth crash peaks in $T_{\mathrm{C+4}}$ seem to grow somewhat toward the end of the OPCD pulse, in conjunction with the lower I_{p} and n_{e},

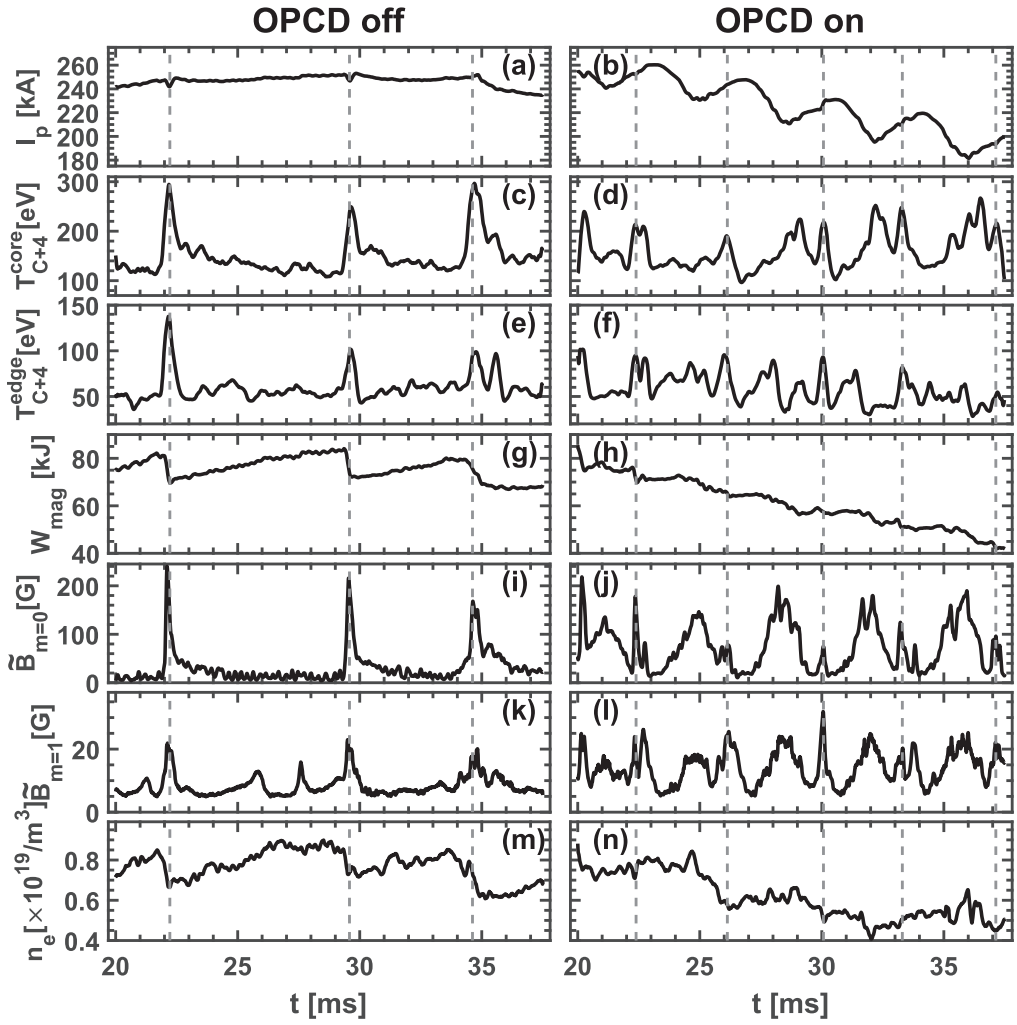

Figure 6. Time evolution during a standard, OPCD off discharge at $\langle F \rangle \approx -0.35$ (left column) and an OPCD pulse at $f_{osc} = 275$ Hz, full-amplitude $A_{osc} \approx 0.35$, and $\langle F \rangle \approx -0.35$ (right column): (a), (b) plasma current I_p; (c), (d) core- ($r/a = +0.11$) and (e), (f) edge-chord ($r/a = -0.76$) C^{+4} impurity ion temperature T_{C+4}; (g), (h) equilibrium magnetic energy W_{mag}; (i), (j) $m = 0$ ($1 \leqslant n \leqslant 4$) and (k), (l) $m = 1$ ($5 \leqslant n \leqslant 15$) edge magnetic fluctuation amplitudes $\widetilde{B}_{m=0}$ and $\widetilde{B}_{m=1}$; (m), (n) central chord-average electron density n_e.

although a robust empirical phenomenon is not clear from the data we have collected.

In the same way as that described above, we average over sawtooth crash events for these more deeply reversed plasmas, with the sawtooth ensemble-average results plotted in figure 7. Again showing the correlation between equilibrium magnetic energy loss and ion heating, the crash-specific drop in W_{mag} is smaller for OPCD on than for the standard case, just as the T_{C+4} peak during the crash is smaller. The OPCD case also has a slow drop in W_{mag} about 1 ms before the crash, simultaneous with the upward excursions in $\widetilde{B}_{m=0}$ and $\widetilde{B}_{m=1}$ and in T_{C+4} for the core-chord, in contrast to the standard case for the corresponding time, where W_{mag} is ramping up as $\widetilde{B}_{m=0}$, $\widetilde{B}_{m=1}$, and T_{C+4} are relatively flat. As seen in figure 7, for the edge IDS-II chord, the ensemble-average T_{C+4} excursion between sawteeth is muted, so as to be roughly similar to the standard case.

We observe a clear correlation between electron density n_e and size of reconnection-induced increases in T_{C+4}, as shown in figure 8, which shows ensemble averages of standard RFP and of OPCD cases. For lower density shots ($n_e < 7 \times 10^{18}$ m^{-3}), core-chord T_{C+4} values tend to be around twice as high as they are for higher-density shots ($n_e > 7 \times 10^{18}$ m^{-3}). This seems consistent with the changes in W_{mag} for the respective cases, which are roughly similar to each other for higher and lower densities. In other words, these results suggest that, since similar amounts of liberated magnetic energy are potentially available for ion heating due to reconnection in both cases, the lower density cases will involve larger changes in ion temperature than will the higher-density cases. Note also that of the two OPCD ensembles reflected in figure 8, the lower density case shows a lower time-average W_{mag} than does the higher-density case. This corresponds to the observation that for high-amplitude OPCD at lower density compared to higher-density, the secular ramp-down rate of I_p and therefore W_{mag} is faster, such that lower W_{mag} values are averaged for each successive ensemble time window during the OPCD pulse.

The approximate radial extent of the C^{+4} ion heating we observe is illustrated by a contour map of chord-average

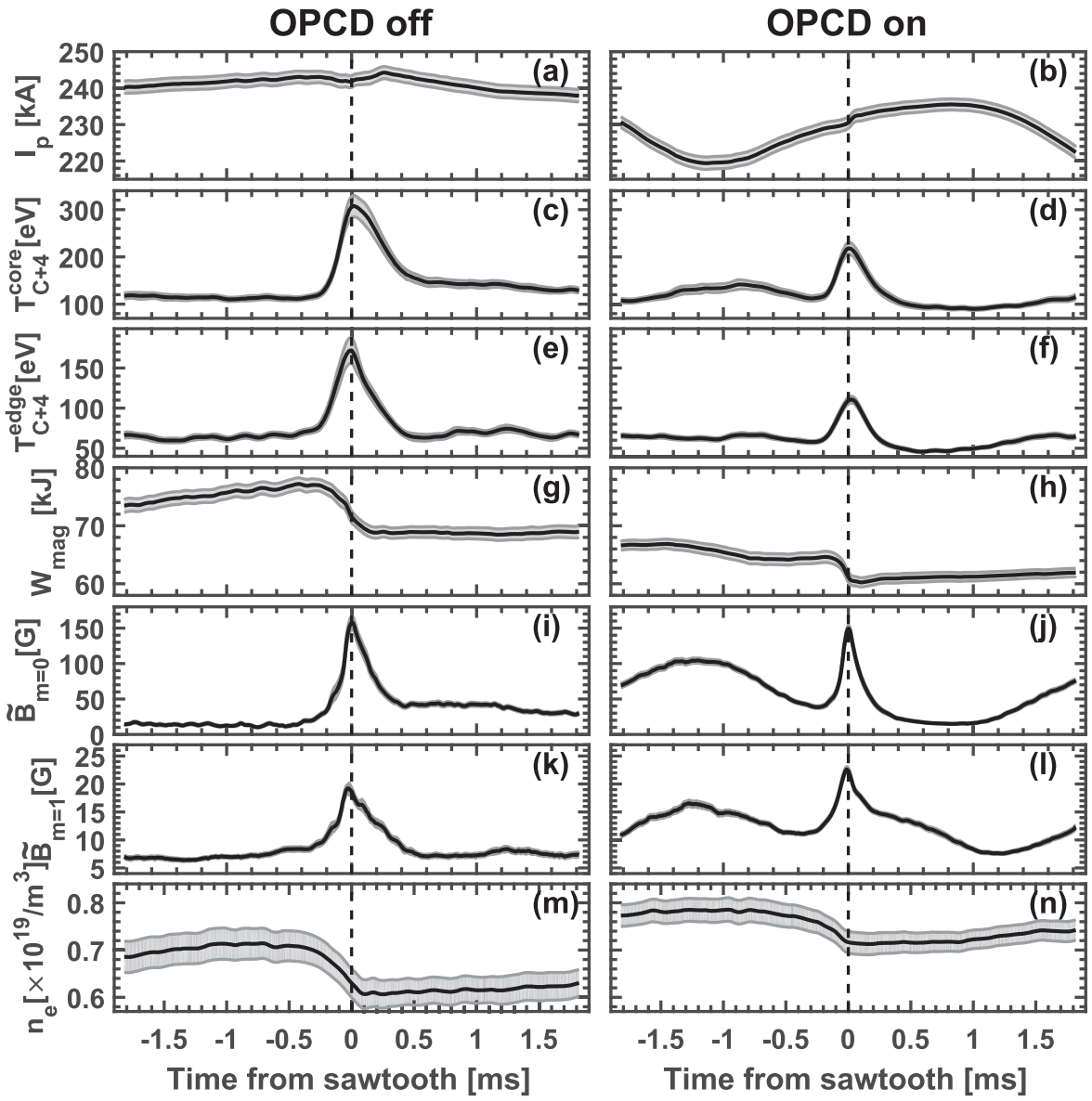

Figure 7. Ensemble-average time evolution during standard, OPCD off discharges at $\langle F \rangle \approx -0.35$ (left column) and OPCD pulses at $f_{osc} = 275$ Hz, full-amplitude $A_{osc} \approx 0.35$, and $\langle F \rangle \approx -0.35$ (right column): (a), (b) plasma current I_p; (c), (d) core- ($r/a = +0.11$) and (e), (f) edge-chord ($r/a = -0.76$) C^{+4} impurity ion temperature T_{C+4}; (g), (h) equilibrium magnetic energy W_{mag}; (i), (j) edge $m = 0$ ($1 \leqslant n \leqslant 4$) and for (k), (l) $m = 1$ ($5 \leqslant n \leqslant 15$) edge magnetic fluctuation amplitudes $\widetilde{B}_{m=0}$ and $\widetilde{B}_{m=1}$; (m), (n) central chord-average electron density n_e. Shaded error bars represent standard errors $\sigma/\sqrt{N}$ of ensemble-average values, where $N = 32$ for OPCD off and 125 for OPCD on.

T_{C+4} versus IDS-II chord impact parameter and shot time, as in figure 9, for an ensemble of eight OPCD shots with a deep reversal of $\langle F \rangle \approx -0.35$, $f_{osc} = 275$ Hz, and full-amplitude $A_{osc} \approx 0.35$. The shots in this ensemble were chosen to have similar plasma densities ($n_e \approx 6 \times 10^{18}$ m^{-3}), and the single IDS-II chord used in this case is changed from inboard $r/a = -0.76$ to outboard $r/a = +0.8$ on a shot-by-shot basis. The arrows indicate average crash times for the ensemble. Modulations of T_{C+4}, both during and between the entrained sawtooth crashes, are visible across the plasma radially from chords centered in the core out to mid-radius. The chord of maximum T_{C+4} modulation, centered at 6 cm outboard of the geometric axis, is near the outboard-shifted plasma magnetic axis. Note that we do not expect OPCD to modulate the Shafranov shift of the magnetic axis by more than a centimeter or so, based on previously reconstructed toroidal equilibria with OFCD oscillations that included similar OPCD amplitudes [30].

Magnetic reconnection in RFPs has previously been observed to anisotropically heat the ions, preferentially increasing $T_\perp$ over $T_\parallel$ with respect to the equilibrium magnetic field [12]. The interpretation of these chord-average signal profiles is complicated by the combination of this anisotropy with the IDS-II diagnostic's preferential detection of $T_\perp$ in the core transitioning to $T_\parallel$ in the edge, with OPCD's modulation

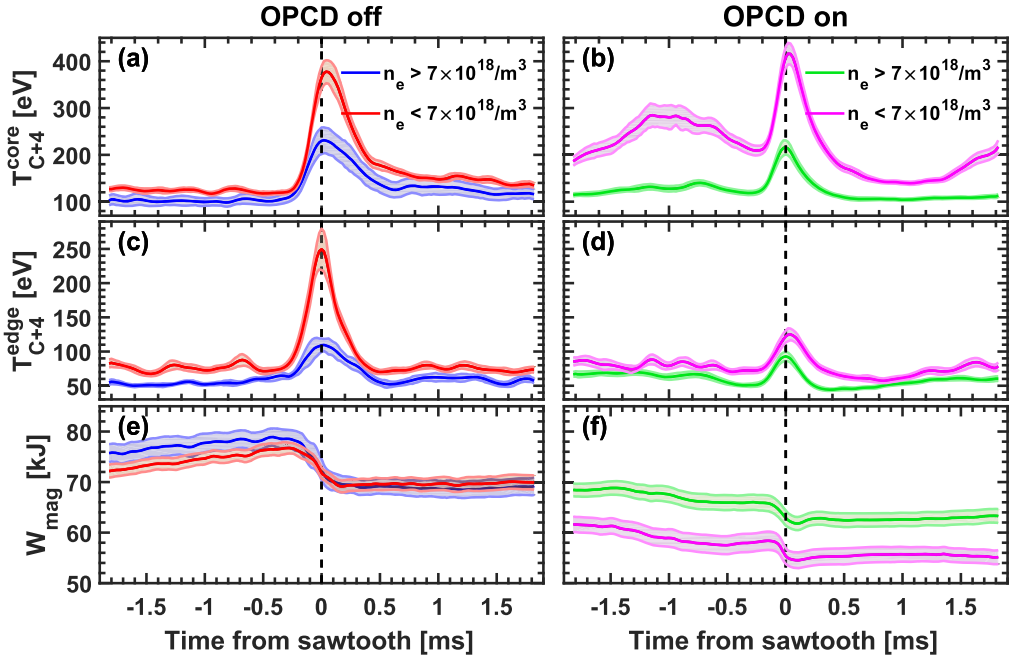

Figure 8. Ensemble-average time evolution during standard, OPCD off discharges at $\langle F\rangle \approx -0.35$ (left column) and OPCD pulses at $f_{osc} = 275$ Hz, full-amplitude $A_{osc} \approx 0.35$, and $\langle F\rangle \approx -0.35$ (right column) for the case of high ($> 7 \times 10^{18}$ m^{-3}) (blue, green) and low ($< 7 \times 10^{18}$ m^{-3}) (red, pink) shot-average electron density n_e: (a), (b) core- ($r/a = +0.11$) and (c), (d) edge-chord ($r/a = -0.76$) C^{+4} impurity ion temperature T_{C+4}; (e), (f) equilibrium magnetic energy W_{mag}. Shaded error bars represent standard errors $\sigma/\sqrt{N}$ of ensemble-average values, where $N = 12$ and 19 for OPCD off at high and low density and 37 and 36 for OPCD on at high and low density, respectively.

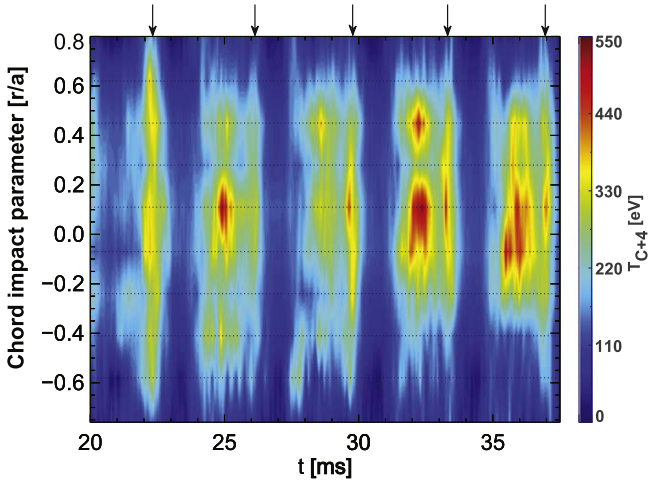

Figure 9. Chord-averaged measurements of C^{+4} impurity ion temperature T_{C+4} versus IDS-II chord impact parameter and time for an ensemble of OPCD shots at $f_{osc} = 275$ Hz, $A_{osc} \approx 0.35$, $\langle F\rangle \approx -0.35$, and $n_e \approx 5.6 \times 10^{18}$ m^{-3}. Positive (negative) r/a positions are outboard (inboard) of the geometric axis. The arrows indicate average crash times for the ensemble.

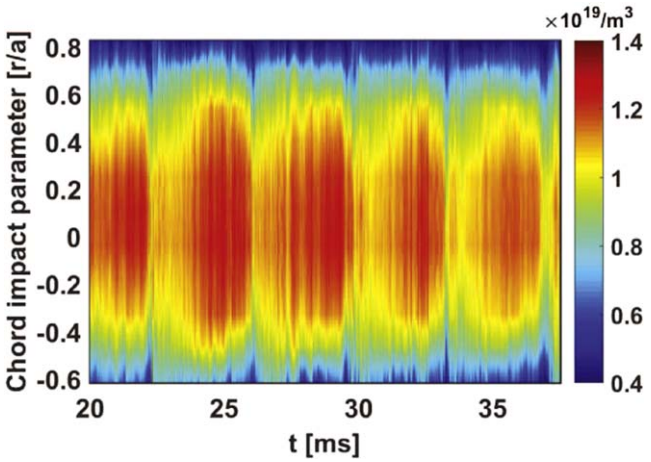

Figure 10. Chord-averaged measurements of electron density n_e versus FIR chord impact parameter and time for a single OPCD pulse. Positive (negative) r/a positions are outboard (inboard) of the geometric axis.

of the equilibrium current profile, and with possible radial profile variations in C^{+4} emissivity.

The electron density n_e profile tends to oscillate at the OPCD frequency. It is otherwise similar to the case of standard RFPs: a broad radial profile and quick drops during sawtooth crashes. An example of chord-average FIR measurements of n_e versus chord impact parameter for a single OPCD pulse is shown in figure 10.

5. Discussion

The application of OPCD to RFP plasmas in MST is observed to modulate global magnetic tearing fluctuations and to entrain the sawtooth relaxation cycle. Thus, the frequency of sawtooth crashes can be modified according to the applied oscillation frequency. In the case of OPCD of sufficient amplitude and a frequency roughly equal to the intrinsic average crash frequency, this makes the otherwise

quasiperiodic sawtooth cycle more strictly periodic. Overall, these effects are ascribed to OPCD's regular modulations of the λ profile, which are comparable in magnitude to the changes due to self-organization in the standard RFP, i.e. the interplay between the steady applied toroidal loop voltage and global magnetic relaxation. In OPCD of sufficient amplitude, the oscillating poloidal loop voltage typically drives the λ profile linearly unstable to $m = 1$ tearing modes, apparently promoting a surge of nonlinearly coupled $m = 0$ and $m = 1$ modes that eventually leads to a sawtooth crash, during a repeatable phase window of each OPCD cycle. The picture that emerges is one of an entrained nonlinear limit cycle rather than merely one of a linear threshold being crossed in a periodic manner. Indeed, while the phase windows for the entrained crashes tend to be quite narrow, there is apparently no direct correlation between reaching linear instability and the moment of crash onset.

Between entrained crashes, OPCD also appears to drive $m = 0$ modes unstable, leading to large amplitudes both for these and for $m = 1$ modes, the latter presumably via nonlinear coupling. Though usually observed to be stable in standard RFPs in MST, $m = 0$ modes can become resistively unstable depending on shell proximity [4] and the features of the edge current or pressure profile [3, 35, 46]. The large λ-profile modulations caused by OPCD are likely behind the apparent $m = 0$ instability between crashes.

Meanwhile, the n spectra of the $m = 1$ excursions between crashes in OPCD, though typically MH, are single-mode-dominated in some circumstances, bearing interesting resemblances to both OPCD results on RFX [22, 23] and some PPCD results on MST [45].

Recall from section 3 that the (Θ, F) trajectories for the standard RFP sawtooth cycle are clockwise, while their full-amplitude OPCD counterparts are observed to be counterclockwise overall, though there is added complexity for different OPCD amplitudes and frequencies. We note that corresponding trajectories for OFCD cases tend to be clockwise for strongly positive net magnetic helicity injection due to OFCD, counterclockwise for strongly negative injection, i.e. strong ejection [35]. Thus, perhaps there is a logical connection between the senses of these cyclic trajectories and the senses of processes related to magnetic relaxation such as helicity injection. To be clear, OPCD alone does not inject net helicity, whose injection rate is $2V_\phi\,\Phi$, with V_ϕ the toroidal loop voltage and Φ the toroidal magnetic flux. Although the oscillating poloidal loop voltage does induce an oscillation in Φ, there is no significant oscillation in V_ϕ.

The application of OPCD is also observed to modulate ion heating in the RFP, evidently by modulating the reconnection activity inherent in simultaneous $m = 0$ and $m = 1$ mode activity. As expected from previous work [7, 14], the measured ion temperature increases are observed to be linked to decreases in equilibrium magnetic energy W_{mag} during relaxation, the ultimate source for the reconnection-based ion heating apparently at work in these experiments. While the drops in W_{mag} characteristic of relaxation are roughly the same at higher or lower plasma densities, we observe markedly larger ion temperature increases at lower densities than at higher densities. The observed impurity ion heating appears to have a broad spatial profile, again similar to the results of previous work on both impurity and majority ion heating during global magnetic reconnection [9], though as described in section 4, interpreting the profile is complicated by several known physical and systematic effects.

OPCD also modulates the plasma current I_{p}, due to the inherent coupling between poloidal and toroidal fields in the RFP. In the MST experiments presented here at large OPCD amplitudes ($A_{\mathrm{osc}} \approx |\langle F \rangle| \approx 0.35$), both I_{p} and the global electron density n_{e} undergo marked secular decreases in addition to their cyclic modulations, and we ascribe this to heat and particle transport effects of the strong tearing mode activity induced and modulated by OPCD. In this context, we note that these large-amplitude experiments show quite different results from those of experiments on RFX [22, 23] in which RFP performance was measurably improved at smaller reported OPCD amplitudes (around $A_{\mathrm{osc}} \approx 0.1$ or lower in the cited cases).

We have not measured electron temperature T_{e} profiles during OPCD in MST using the MST Thomson scattering system [47]. Doing so might provide further insight into the interactions between the applied voltage oscillations, magnetic relaxation, and stochastic transport due to magnetic reconnection, as well as aid understanding of OPCD's effects on RFP performance. Based on previous Thomson measurements during OFCD [30], in OPCD, we might expect some T_{e} oscillation in the core due to Ohmic heating with the oscillating plasma current and perhaps some compressional heating with the oscillating loop voltage, as well as rapid T_{e} drops associated with rapid stochastic electron heat transport during magnetic relaxation, both during and between entrained sawtooth crashes.

More generally, potential future work on the topic of oscillating fields in RFPs will be centered on applying both poloidal and toroidal loop voltage oscillations, i.e. applying OFCD, with dual PPSs. In addition to the toroidal magnetic field PPS used for the work reported in this paper, a new PPS for the poloidal field [36] was recently commissioned on MST, capable of producing a toroidal loop voltage oscillation and enabling OFCD with dual PPSs. This new PPS OFCD capability is much more flexible than the already-existing OFCD tank-circuit system [48], since, within PPS bandwidth limitations, essentially arbitrary oscillating waveforms are possible, and in particular, those with easily adjustable frequencies, as presented for OPCD in this paper.

Experimental results from the tank-circuit system [35] as well as numerical results from nonlinear MHD simulations [49] suggest that the precisely controlled application of both OFCD oscillations may provide a powerful means of control over RFP dynamics. This could be useful for further, more precise studies of reconnection onset. For example, using both poloidal and toroidal oscillators, it might be possible to control the (Θ, F) trajectory to aid in examining the contributions of nonlinear mode coupling [5] or to probe for hypothetical dependences of crash triggering on linear

stability [43]. Such laboratory experiments could help shed light on the issues of onset and triggering in space and astrophysical contexts [34].

Comprehensive waveform control might also prove advantageous to the RFP fusion development path. For instance, generalized applied loop voltages may allow effective control over magnetic relaxation activity in the RFP [50, 51] simultaneous with helicity injection as in OFCD. Such innovations might also apply to other magnetic confinement configurations.

In summary, these OPCD experiments show that the application of oscillating poloidal loop voltages to the RFP modifies the behavior of both core- and edge-resonant tearing modes, apparently by affecting their linear stability and their mutual nonlinear coupling, as it moves the plasma equilibrium in (Θ, F) trajectories distinct from those in the standard RFP. This process entrains and modifies the sawtooth cycle and leads to energy exchange via magnetic reconnection that produces modulated impurity ion heating.

The numerical data presented in this paper is available in the supplementary material (available online at stacks.iop.org/ppcf/61/045004/mmedia).

Acknowledgments

This material is based upon work supported by the U.S. Department of Energy Office of Science, Office of Fusion Energy Sciences program under Award Numbers DE-FC02-05ER54814 and DE-SC0018266. Z Li was supported by the National Natural Science Foundation of China (Nos. 11635008 and 11775220) and China Scholarship Council (201606340122).

ORCID iDs

Zichao Li https://orcid.org/0000-0002-6695-6940

References

[1] Bodin H A B and Newton A A 1980 *Nucl. Fusion* **20** 1255
[2] Dexter R N, Kerst D W, Lovell T W, Prager S C and Sprott J C 1991 *Fusion Technol.* **19** 131
[3] Choi S, Craig D, Ebrahimi F and Prager S C 2006 *Phys. Rev. Lett.* **96** 145004
[4] Jiang Z X, Bondeson A and Paccagnella R 1995 *Phys. Plasmas* **2** 442
[5] Ho Y L and Craddock G G 1991 *Phys. Fluids* B **3** 721
[6] Ji H, Prager S C and Sarff J S 1995 *Phys. Rev. Lett.* **74** 2945
[7] Fiksel G, Almagri A F, Chapman B E, Mirnov V V, Ren Y, Sarff J S and Terry P W 2009 *Phys. Rev. Lett.* **103** 145002
[8] Gangadhara S, Craig D, Ennis D A, Den Hartog D J, Fiksel G and Prager S C 2007 *Phys. Rev. Lett.* **98** 075001
[9] Gangadhara S, Craig D, Ennis D A, Den Hartog D J, Fiksel G and Prager S C 2008 *Phys. Plasmas* **15** 056121
[10] Howell R B and Nagayama Y 1985 *Phys. Fluids* **28** 743
[11] Hsu S C, Carter T A, Fiksel G, Ji H, Kulsrud R M and Yamada M 2001 *Phys. Plasmas* **8** 1916–28
[12] Magee R M, Hartog D J D, Kumar S T A, Almagri A F, Chapman B E, Fiksel G, Mirnov V V, Mezonlin E D and Titus J B 2011 *Phys. Rev. Lett.* **107** 065005
[13] Kumar S T A, Almagri A F, Craig D, Den Hartog D J, Nornberg M D, Sarff J S and Terry P W 2013 *Phys. Plasmas* **20** 056501
[14] Cartolano M S, Craig D, Den Hartog D J, Kumar S T A and Nornberg M D 2014 *Phys. Plasmas* **21** 012510
[15] Yamada M, Yoo J and Myers C E 2016 *Phys. Plasmas* **23** 055402
[16] Sarff J S, Hokin S A, Ji H, Prager S C and Sovinec C R 1994 *Phys. Rev. Lett.* **72** 3670
[17] Bartiromo R, Martin P, Martini S, Bolzonella T, Canton A, Innocente P, Marrelli L, Murari A and Pasqualotto R 1999 *Phys. Rev. Lett.* **82** 1462
[18] Yagi Y, Koguchi H, Hirano Y, Shimada T, Sakakita H, Sekine S, Chapman B E and Sarff J S 2003 *Phys. Plasmas* **10** 2925
[19] Cecconello M, Malmberg J A, Spizzo G, Chapman B E, Gravestjin R M, Franz P, Piovesan P, Martin P and Drake J R 2003 *Plasma Phys. Control. Fusion* **46** 145
[20] Chapman B E *et al* 2001 *Phys. Rev. Lett.* **87** 205001
[21] Chapman B E *et al* 2010 *Plasma Phys. Control. Fusion* **52** 124048
[22] Bolzonella T, Martin P, Martini S, Marrelli L, Pasqualotto R and Terranova D 2001 *Phys. Rev. Lett.* **87** 195001
[23] Terranova D, Alfier A, Bonomo F, Franz P, Innocente P and Pasqualotto R 2007 *Phys. Rev. Lett.* **99** 095001
[24] Ciaccio G, Veranda M, Bonfiglio D, Cappello S, Spizzo G, ChaconL L and White R B 2013 *Phys. Plasmas* **20** 062505
[25] Bevir M K, Gimblett C G and Miller G 1985 *Phys. Fluids* **28** 1826
[26] Boozer A H 1986 *Phys. Fluids* **29** 4123
[27] Ebrahimi F, Prager S C, Sarff J S and Wright J C 2003 *Phys. Plasmas* **10** 999
[28] Schoenberg K F *et al* 1988 *Phys. Fluids* **31** 2285
[29] McCollam K J, Blair A P, Prager S C and Sarff J S 2006 *Phys. Rev. Lett.* **96** 035003
[30] McCollam K J *et al* 2010 *Phys. Plasmas* **17** 082506
[31] Najmabadi F *et al* 1993 *Fusion Eng. Des.* **23** 69
[32] Sarff J S 2007 A hybrid inductive scenario for a pulsed-burn RFP reactor with quasi-steady current *12th IEA RFP Workshop (Kyoto)*
[33] Sarff J S 2008 *J. Plasma Fusion Res.* **84** 800
[34] Zweibel E G and Yamada M 2016 *Proc. R. Soc.* A **472** 20160479
[35] McCollam K J, Holly D J, Mirnov V V, Sarff J S and Stone D R 2012 AC loop voltages and MHD stability in RFP plasmas *54th Annual Meeting of the APS Division of Plasma Physics, JP8 150*
[36] Holly D J, Adney J R, McCollam K J, Morin J C and Thomas M A 2011 Programmable power supply for MST's poloidal field *IEEE/NPSS 24th Symp. on Fusion Engineering, SP3-47*
[37] Craig D, Den Hartog D J, Ennis D A, Gangadhara S and Holly D 2007 *Rev. Sci. Instrum.* **78** 013103
[38] Brower D L, Ding W X, Terry S D, Anderson J K, Biewer T M, Chapman B E, Craig D, Forest C B, Prager S C and Sarff J S 2003 *Rev. Sci. Instrum.* **74** 1534
[39] Antoni V, Merlin D, Ortolani S and Paccagnella R 1986 *Nucl. Fusion* **26** 1711
[40] Stoneking M R, Chapman J T, Den Hartog D J, Prager S C and Sarff J S 1998 *Phys. Plasmas* **5** 1004
[41] Cappello S and Biskamp D 1996 *Nucl. Fusion* **36** 571

[42] Sarff J S *et al* 1995 *Phys. Plasmas* **2** 2440
[43] Kusano K and Sato T 1990 *Nucl. Fusion* **30** 2075
[44] Ott E 2002 *Chaos in Dynamical Systems* (Cambridge: Cambridge University Press)
[45] Marrelli L, Martin P, Spizzo G, Franz P, Chapman B E, Craig D, Sarff J S, Biewer T M, Prager S C and Reardon J C 2002 *Phys. Plasmas* **9** 2868
[46] Zanca P and Terranova D 2006 *Plasma Phys. Control. Fusion* **48** 407
[47] Reusch J A, Borchardt M T, Den Hartog D J, Falkowski A F, Holly D J, O'Connell R and Stephens H D 2008 *Rev. Sci. Instrum.* **79** 10E733
[48] Nonn P D, Blair P D, McCollam K J, Sarff J S and Stone D R 2011 *Rev. Sci. Instrum.* **82** 064701
[49] Ebrahimi F and Prager S C 2004 *Phys. Plasmas* **11** 2014
[50] Nebel R A, Schnack D D and Gianakon T A 2002 *Phys. Plasmas* **9** 4968
[51] Zanca P 2007 *Plasma Phys. Control. Fusion* **49** 113